Tapered lateral flow immunoassay based point-of-care diagnostic device for ultrasensitive colorimetric detection of dengue NS1

Sanjay Kumar,[1] Pulak Bhushan,[1] Vinay Krishna,[2] and Shantanu Bhattacharya[1,3,a)]

[1]*Microsystems Fabrication Laboratory, Department of Mechanical Engineering, Indian Institute of Technology Kanpur, Kanpur, Uttar Pradesh 208016, India*
[2]*Department of Cardiology, LPS Institute of Cardiology, G.S.V.M. Medical College, Kanpur, Uttar Pradesh 208016, India*
[3]*Design Programme, Indian Institute of Technology Kanpur, Kanpur, Uttar Pradesh 208016, India*

(Received 13 April 2018; accepted 30 April 2018; published online 14 May 2018)

Dengue virus, a *Flaviviridae* family member, has emerged as a major worldwide health concern, making its early diagnosis imperative. Lateral flow immunoassays have been widely employed for point-of-care diagnosis of dengue because of their rapid naked eye readouts, ease of use, and cost-effectiveness. However, they entail a drawback of low sensitivity, limiting their usage in clinical applications. Herein, we report a novel lateral flow immunoassay for detection of dengue leveraging on the benefits of gold decorated graphene oxide sheets as detection labels and a tapered nitrocellulose membrane. The developed assay allows for rapid (10 min) and sensitive detection of dengue NS1 with a detection limit of 4.9 ng mL^{-1}, ~11-fold improvement over the previously reported values. Additionally, the clinical application of the developed assay has been demonstrated by testing it for dengue virus spiked in human serum. The reported lateral flow immunoassay shows significant promise for early and rapid detection of several target diseases. *Published by AIP Publishing*. https://doi.org/10.1063/1.5035113

I. INTRODUCTION

Dengue is one of the fastest emerging arthropod-borne viral diseases spreading worldwide, especially in the tropical and subtropical countries. The dengue viruses comprise four distinct serotypes (DENV-1, DENV-2, DENV-3, and DENV-4), which belong to the *flavivirus* genus in the family *Flaviviridae*.[1] A mature dengue virion (40–50 nm diameter, spherical shape) contains a positive-sense single-strand RNA genome enclosed by an isometric or icosahedral nucleocapsid enveloped with a lipopolysaccharide.[2–4] Each genome is about 11 kb in length and encodes three structural proteins [the nucleocapsid (C), membrane (M), and envelope (E) glycoproteins] and seven nonoverlapping, non-structural proteins (NS1, NS2A, NS2B, NS3, NS4A, NS4B, and NS5).[3] The dengue virus is transmitted to human beings via the bite of an infected female mosquito, *Aedes aegypti* or *Aedes albopictus*. The infection from the dengue virus causes clinical syndromes ranging from self-limiting dengue fever (DF) to life-threatening dengue haemorrhagic fever/dengue shock syndrome (DHF/DSS). Over the past few decades, the incidence of dengue infection has risen rapidly. An early diagnosis of dengue virus is imperative for better clinical management, etiological investigation, surveillance, and disease control. NS1, a highly conserved glycoprotein, has emerged as a major antigenic biomarker for early detection of dengue. Studies on dengue virus have revealed that NS1 is dominant in the early days of the illness. The NS1 concentration is low over the first two days, but increases rapidly with the

a)Author to whom correspondence should be addressed: bhattacs@iitk.ac.in Tel: +91-512-2596056 (Office)

increasing number of days peaking at day 4. The reported NS1 serum levels ranged from 0.04 to 2 μg mL^{-1} in patients with primary infection and from 0.01 to 2 μg mL^{-1} in patients with secondary infection. Further, the levels of NS1 circulating in the bloodstream of DENV-1 infected patients are estimated to range from 0.01 to 50 μg mL^{-1}.[5]

The requirement to elicit early diagnostic techniques for dengue has been a major challenge. Currently, laboratory-based reverse-transcription polymerase chain reaction (RT-PCR)[6] and antigen capture-enzyme linked immunosorbent assay[1,2] are used for diagnosis of dengue. These techniques are highly accurate but are expensive, have slow turnaround time, and require sophisticated process. In the recent years, several biosensors have been developed for rapid detection of NS1, such as enzyme immunoassay,[7] long-range surface plasmon waveguides,[8] electrochemical lateral flow immunosensors,[9] and colorimetric sensors.[10,11] Among these, colorimetric sensors exhibit significant advantages such as simplicity, real time naked eye detection, and no external power requirement. This has led to the development of lateral flow immunoassays based on colorimetric detection schemes, as an alternative to the conventional laboratory based assays. These lateral flow devices have been widely employed as point-of-care screening tools for rapid detection of dengue.[10,12–14] They are made of cellulose-based paper utilizing either chromatographic paper or nitrocellulose (NC) membrane. Colloidal metal nanoparticles such as gold (Au) and silver (Ag) are exploited as detection labels owing to their monodispersive size, ease of functionalization with antibodies/antigens, high stability, and tunable optical properties.[15–17] The ease of use and low cost of these lateral flow assays make them particularly attractive for rapid and sensitive diagnostics.

While the current lateral flow based colorimetric biosensors are robust and inexpensive, various limitations such as poor sensitivity, specificity, and high limit-of-detection (LOD) are associated with these devices.[18] One of the major reasons for the high LODs is the tendency for destabilized self-aggregation of plasmonic metal nanoparticles. As a consequence of this aggregation, the number of active binding sites for antibody immobilization decreases, leading to a low sensitivity. In order to prevent this, metal nanoparticles have been anchored on specific supports. Recently, reduced graphene oxide (rGO), a monolayer of two-dimensional carbon-based materials, has been extensively employed as an anchoring substrate for several nanoparticles, for preparation of nanocomposites such as Ag-rGO, Au-rGO, etc. Distinguished properties like hydrophilicity, high surface area, versatile surface modification, rapid electron transfer capability, biocompatibility, and photoluminescence make reduced graphene oxide a pragmatic tool in the field of medical diagnostics and biosensing.[19–21] Further, several architectural modifications to the conventional lateral flow immunoassays have been employed to improve the sensitivity. For instance, creating polydimethylsiloxane barriers or wax pillars on the NC membrane[22,23] or adding a sponge following the conjugate pad (CP)[24] allows for effective flow control, however adds to the overall cost of the device. Alternatively, concentration gradient at the test line can be tuned by the shape of the NC membrane. A modification of such manner could be a simpler approach over the previously reported techniques for potential improvement in the sensitivity at a minimal cost.

In this work, we developed a simple, highly sensitive, and low-cost lateral flow immunoassay for early detection of dengue NS1 in human serum. We demonstrate for the first time introduction of a tapered NC membrane, simultaneously leveraging on the benefits of Au-rGO as a detection label. Gold nanoparticles anchored on rGO sheets have been utilized for labelling, enabling the device to exhibit high sensitivity levels. The high surface-to-volume ratio offered by the rGO sheets inhibits gold nanoparticle aggregation, increasing the number of active binding sites for immobilization of the anti-dengue antibodies. Further, an interesting architectural approach was employed wherein a modified tapered NC membrane was used. The modification led to an increase in the concentration gradient of the antigen bound nanoparticles at the test line, thus increasing the color intensity at the test line. This substantial signal enhancement translated into achieving an extremely low detection limit of 4.9 ng mL^{-1}. The taper angle of the NC membrane has been optimized to achieve this high level of analytical sensitivity. Together, an assay exploiting the superior physical and chemical properties of Au-rGO nanocomposite along with architectural modifications yields a ~11-fold increase in the device

sensitivity as compared to the conventional lateral flow assays. We envision that the proposed assay can establish a significant advancement in the area of point-of-care disease diagnostics enabling sensitive and accurate detection.

II. EXPERIMENTAL

A. Materials and reagents

Gold(III) chloride trihydrate ($HAuCl_4 \cdot 3H_2O, \geq 99.9\%$), sulphuric acid ($H_2SO_4, \geq 98\%$), sodium chloride (NaCl), graphite flakes (acid treated, $\geq 99\%$), potassium permanganate ($KMnO_4, \geq 99\%$), hydrochloric acid (35%), potassium chloride, monopotassium phosphate ($KH_2PO_4, \geq 99\%$), disodium phosphate ($Na_2HPO_4, \geq 99\%$), tri-sodium citrate dihydrate ($C_6H_5Na_3O_7 \cdot 2H_2O, \geq 99\%$), hydrogen peroxide (30 wt. % in H_2O), HEPES ($C_8H_{18}N_2O_4S$), poly(ethylene glycol) (PEG, 8 kDa), poly(ethylene glycol) methyl ether (mPEG-SH, 5 kDa), sodium periodate ($NaIO_4, \geq 99.8\%$), and Whatman qualitative filter paper grade 1 were obtained from Sigma Aldrich, India. High performance liquid chromatography (HPLC) and Milli-Q ultrapure water were used for preparation of all aqueous solutions. Mouse dengue NS1 monoclonal detection antibody (No. MBS832514, >90%), mouse dengue NS1 monoclonal capture antibody (No. MBS834562, >90%), goat anti-mouse IgG secondary antibody (No. MBS330167, >90%) and dengue virus (DENV-NS1 serotype 1) recombinant antigen (No. MBS569085, $\geq 95\%$), plasmodium falciparum HRP2, recombinant protein (MBS232321), and plasmodium vivax, Recombinant Protein (MBS328042) were purchased from MyBioSource, Inc. USA. Hydrazide (semicarbazide) (dithiolaromatic PEG6-NHNH2, No. SPT-0014B) was purchased from Sensopath Technologies, USA. Sample pad (No. CF3), conjugate pad (No. standard 14), and nitrocellulose membrane (No. FF120HP) were purchased from GE healthcare, India. SuperBlock™ (PBS) Blocking Buffer (No. 37515) was obtained from ThermoFisher Scientific, India. All experiments were performed in compliance with the relevant laws and national guidelines (Ethical Guidelines for Biomedical Research on Human Participants, provided by Indian Council of Medical Research), and the ethical clearance for the same was provided by the GSVM Medical College, Kanpur.

B. Synthesis of gold-graphene oxide (Au-rGO) nanocomposites

First, graphene oxide (GO) was synthesized using modified Hummer's method.[25] Next, reduced GO was prepared by first, suspending 50 mg of as-prepared GO in 200 mL of Milli-Q ultrapure water. After rigorous stirring and ultrasonication for 30 min, 50 μL of hydrazine monohydrate solution was gradually added. The resulting mixture was heated in a water bath at 80 °C for 4h. The resulting suspension was then filtered using Whatman filter paper, washed several times with milli-Q ultrapure water, and vacuum dried at 50 °C to obtain rGO. Gold nanoparticles (AuNPs) of size 40 nm were synthesized using the seeded growth strategy.[26] The final Au-rGO nanocomposites were prepared by an *ex-situ* process. In brief, 1 mL of ultrasonically dispersed rGO (0.3 mg mL^{-1}) and 20 mL of as-prepared AuNP solution ($\sim 7.6 \times 10^{10}$ particles mL^{-1}) were mixed and diluted in 20 mL of HPLC water. The mixture was then kept at room temperature for 24 h under constant stirring. The obtained colloidal Au-rGO solution was filtered and washed several times with HPLC water for residue removal. The final product was stored at 4 °C until use.

C. Antibody conjugation to gold-graphene oxide nanocomposites (Au-rGO-Ab)

Directional conjugation[27] was used for conjugation of detection antibodies to the Au-rGO nanocomposites. First, linker hydrazide (semicarbazide) was attached to the detection antibody. In the process, 100 μL of detection antibody solution (1 mg mL^{-1}) and 10 μL of $NaIO_4$ were added to a Na_2HPO_4 (100 mM) solution and incubated in dark for 30 min at room temperature. Then, 2 mL of linker solution (46.5 mM) was added to the above solution and further incubated for 1 h. The solution was then filtered using centrifugation at 2000g for 10 min at 4 °C. The supernatant was discarded and the retained solution was resuspended in 1 mL of HEPES

(40 mM). To conjugate the antibodies to the Au-rGO nanocomposites, 100 μL of antibody-linker solution (100 μg mL^{-1}) was diluted in 500 μL of 1 × PBS (pH 7.4) and mixed with 1 mL of Au-rGO solution for 20 min at room temperature. Next, 100 μL of mPEG-SH (10^{-5} M) was added to the above solution and stirred (at 200 rpm) for 20 min at room temperature followed by an addition of 100 μL of 2% PEG solution in 1 × PBS. A backfill of thiolated PEG is used to reduce fouling and non-specific nanoparticle-Ab and Ab-Ab interactions.[28] The resulting solution mixture was then centrifuged at 2500g for 30 min at 4 °C. The supernatant was discarded and the remaining solution was resuspended in 1 mL of 2% PEG solution in 1 × PBS.

D. Characterization

The UV-visible spectra (UV-Vis) were acquired with an Evolution 300 spectrophotometer (Thermo Scientific). High resolution transmission electron microscope (HR-TEM) images were recorded on a FEI Titan G2 60-300 TEM operated at 300 kV. Raman spectra were obtained using a confocal Raman microscope with 10× objective using an excitation He-Ne laser light of wavelength 532 nm. A Bruker D8 Advance X-ray diffractometer with Cu Ka (k = 0.154 nm) radiation (Bruker AXS, Germany) was utilized for performing X-ray diffractometry (XRD). Fourier transform infrared spectroscopy (FTIR) was carried out on a PerkinElmer Spectrum Version 10.03.06. Zeta potential measurements were performed on a Beckman Coulter Delsa Nano C. Fluorescence spectroscopy was carried out on a PerkinElmer LS 55 fluorescence spectrometer. The pH values of the buffer solutions were recorded using a Labman benchtop pH meter. ImageJ software was used for image analysis of the TEM and test strip images. Photographs of the samples in vials and on test strips were taken using a mobile phone camera.

E. Quantitation of immobilized antibodies on Au-rGO nanocomposites

The number of immobilized antibodies per AuNP was estimated through fluorescence spectroscopy. First, a stock solution of fluorescein isothiocyanate (FITC) was prepared in 0.1 M sodium carbonate-bicarbonate buffer (pH 9). Next, 0.5 mL of antibody-linker solution of different concentrations (25, 50, 75, and 100 μg mL^{-1}) was added dropwise to 2 mL of as-prepared FITC solution in a vial and vortexed until the FITC reagent was dissolved. The mixture was incubated for 2 h at room temperature with mild stirring in dark light. The reaction mixture was then centrifuged at 1000g for 5 min at 4 °C and the supernatant was discarded. These FITC tagged antibodies were mixed with 1 mL of Au-rGO solution and incubated for 20 min at room temperature. The as-prepared solution was used for carrying out the fluorescence spectroscopy measurements. Using these measurements, a linear calibration curve was established between the fluorescence intensity (at 519 nm) and the concentration of labeled antibodies. Next, the solution was centrifuged for 30 min at 2500g at 4 °C and the supernatant was extracted and further used for measuring its fluorescence intensity. The concentration of unbounded antibodies in the supernatant was determined using the developed calibration curve. The final concentration of antibodies attached to the nanocomposites was obtained by subtracting the concentration of unbounded antibodies in the supernatant from the initial concentration of the labeled antibodies. Due to the linker attachment to the AuNPs, it is convenient to assume that maximum antibodies attach to the gold nanoparticles albeit the non-specific adsorption of a few antibodies to the rGO sheets. Hence, the number of antibodies attached to each nanoparticle was estimated by dividing the total concentration of antibodies with the concentration of gold nanoparticles (7.6×10^{10} particles mL^{-1}).

F. Detection mechanism

A typical lateral flow device consists of four parts namely, sample pad (SP), conjugate pad (CP), nitrocellulose (NC) membrane with test line (T) and control line (C) and absorbent pad (AP) [Fig. 1(a)]. In this sandwich assay format, the sample is loaded onto the SP after which it subsequently migrates to other parts of the test strip. First, at the CP, NS1 antigen (Ag) interacts with the immobilized Au-rGO-Ab conjugates, resulting in the beginning of Au-rGO-Ab-Ag complex formation. The concentration of these complexes increases as they wick through the nitrocellulose

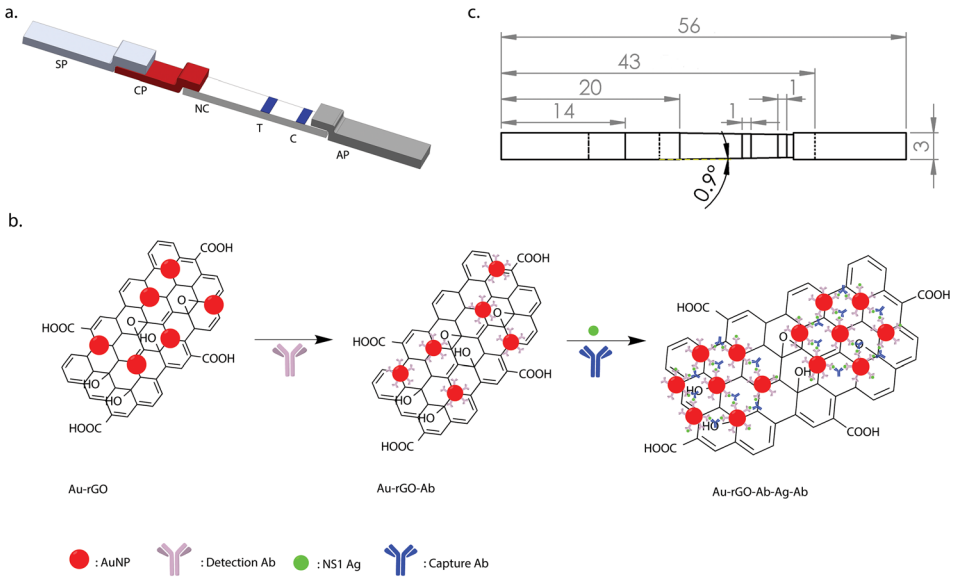

FIG. 1. Device for the lateral flow immunoassay. (a) Schematic of the lateral flow immunoassay. SP: sample pad, CP: conjugate pad, NC: nitrocellulose membrane, T: test line, C: control line, AP: absorbent pad. (b) Detection scheme of dengue detection based on nanoparticle aggregation. (c) The respective dimensions of the immunoassay represented in millimeters (mm).

membrane by capillary action. On reaching the test line, the complexes are captured by the capture antibodies resulting in the formation of a sandwich (Au-rGO-Ab-Ag-Ab) producing a colored band on the strip. If Ag is not present in the sample, no sandwich is formed and no colored band is observed. The excess labeled antibody conjugates then move towards the control line where they are captured by the secondary antibodies. The secondary antibodies bind to the Fc region of the detection antibodies creating a colored band confirming the successful completion of the assay. Further, the excess buffer and the unbounded conjugated nanoparticles are soaked by the absorbent pad. Figure 1(b) shows a schematic of the sandwich format for the lateral flow immunoassay.

G. Lateral flow device design

The overall objective was to develop and validate a low-cost paper-based rapid platform for detection of dengue NS1 at low concentrations. The approach centers on using a tapered NC membrane to improve the sensitivity by enhancing the overall test line signal intensity. To reveal the underlying signal enhancement mechanism of the tapered NC membrane, a mathematical model is developed. On the basis of the convection-diffusion mass balance equation, the test line is optimized, following which Darcy's law and Fick-Jacobs equation of diffusion are utilized to model the flow through the tapered membrane.

A lateral flow assay is based on the immunoreaction between the antigen (A) and Au-rGO-Ab (P). The analytical sensitivity of an assay depends on the concentration of the complex PA reaching the test line, which is governed by the immunoreaction time given to form this complex. The concentration of PA varies as it flows from CP to the test line based on the convection-diffusion mass balance equation[29]

$$\frac{\partial [PA]}{\partial t} = D\frac{\partial^2 [PA]}{\partial X^2} - u\frac{\partial [PA]}{\partial X} + k_a[A][P] - k_d[PA], \tag{1}$$

where D is the molecular interdiffusion coefficient, X is the distance from the start of conjugate pad to the start of the test line, u is the average fluid velocity, and k_a and k_d are association and dissociation rate constants, respectively. The square brackets denote the concentrations of the various species. The above equation can be solved using the initial condition, $[PA]_{X,0} = 0$

and the boundary conditions, $[PA]_{0,t} = 0$ at $X = 0$ and $\partial[PA]/\partial X = 0$; for $X = ut$. The capillary flow time for CP and NC membrane is assumed to be the same to simplify calculations. On substituting the values of the constants in the equation ($A_0 = 100\,nM$, $P_0 = 100\,nM$, $k_a = 6.4 \times 10^5\,(Ms)^{-1}$, $k_d = 10^{-3}\,s^{-1}$, $D = 2 \times 10^{-2}\,m^2\,s^{-1}$, capillary flow time = 200 s/4 cm), the variation of [PA] with distance along the NC membrane is plotted (Fig. S1). The test line distance is optimized such that sufficient reaction time is given to the PA complex to achieve equilibrium concentration, since after that no change in [PA] occurs. This concentration is determined to be 7.5 nM using the following equation:[29]

$$[PA]_{eq} = 0.5 \times \left([A_0] + [P_0] + k_{d1}/k_{a1} - \sqrt{\left([A_0] + [P_0] + k_{d1}/k_{a1}\right)^2 - 4[A_0][P_0]} \right). \tag{2}$$

The optimized test line distance is then the point of intersection with equilibrium concentration of PA and is found to be 2.5 cm from start of CP. However at a lower antigen concentration, the equilibrium concentration of PA is reached at a much shorter distance (1.7 cm for $[A_0] = 5\,nM$). After reaching this distance, the [PA] decreases from this equilibrium concentration as it moves to the test line due to diffusion through the NC membrane. A tapered NC membrane is utilized here to allow for a significant increase in the [PA] reaching the test line, to improve the signal intensity. The signal enhancement as a result of this taper is modeled using Darcy's law and Fick-Jacobs equation of diffusion. Darcy's law was used to demonstrate the fluid transport through the membrane as

$$Q = -\frac{K\,w(x)h}{\mu L}\Delta P \Longrightarrow \Delta P = \frac{Q\mu}{k}\int_0^L \frac{dx}{A(x)}, \tag{3}$$

where Q is the volumetric flow rate, K is the permeability of the NC membrane, x is the position measured from the end of CP, A(x) is the cross-sectional area of the paper strip at position x, h is the cross-sectional area perpendicular to the flow that varies along the flow path, μ is the fluid viscosity, and ΔP is the pressure difference along the length (L) of the membrane. The viscosity[30] ($\sim 2 \times 10^{-3}$ Pa s) and density[31] (1.02 g mL^{-1}) of the fluid were taken to be the same as human serum. Using a known sample volume (150 μL), inlet cross-section, and the fluid absorption time, the inlet velocity was estimated. Atmospheric pressure was taken at the outlet and the sidewalls were under no-slip condition. The permeability (K) of NC membrane was calculated through the Kozeny-Carman equation[22,32]

$$K = \frac{d^2\varepsilon^3}{180(1-\varepsilon)^2}, \tag{4}$$

where d(=0.9 μm) is the average pore diameter of the NC membrane and ε is the porosity of the NC membrane. The permeability of NC membrane was calculated to be 2.33×10^{-16} m^2. Further, the porosity of the membrane was obtained empirically to be 0.34 using

$$\varepsilon = \frac{v_p}{v_p + v_m}, \tag{5}$$

where v_p, v_m are the pore volume and initial volume of NC membrane, respectively. Pore volume was calculated by measuring the change in a known volume of PBS (density = 1.95 g mL^{-1}) after dipping the NC membrane in it.[33] Next, the Fick-Jacobs equation for diffusion was used to evaluate the concentration gradient along the membrane of varying width.[34] The Fick-Jacobs law for diffusion may be expressed as

$$\frac{\partial C(x,t)}{\partial t} = \frac{\partial}{\partial x}\left[D\,A(x)\frac{\partial}{\partial x}\left(\frac{C(x,t)}{A(x)}\right)\right], \tag{6}$$

where C(x, t) is the local concentration of PA complex at location x and time t. COMSOL Multiphysics 5.2 was then used to carry out the finite element modeling based on the above mathematical model. Figure S2(a) reveals the change in concentration as the reagent flows from the conjugate pad to the test line. It is discerned that the concentration of the reagent achieved at the test line is significantly higher for a tapered membrane compared to a straight NC membrane [Fig. S2(b), supplementary material]. Next, validation experiments were carried out to optimize the taper angle of the membrane. Test strips at different taper angles (0°, 0.3°, 0.5°, 0.7°, 0.9°, and 1.1°) were tested at an NS1 concentration of 25 ng mL^{-1}. The sensitivity was estimated by taking an average of the three replications performed for each experiment.

H. Test strip preparation

To prepare the test strip for detection of dengue NS1, first, sample pad and absorbent pad were washed in hot HPLC water (80 °C) and dried in an oven at 37 °C for 2 h. Next, the Au-rGO-Ab conjugates were loaded on the conjugate pad by immersing the pad into the conjugate solution followed by vacuum drying at 37 °C for 2 h on a non-absorbent surface. The dried conjugate pad was stored at <15% relative humidity at 4 °C until use. Capture antibody (0.1 mg mL^{-1}) and secondary antibody (0.1 mg mL^{-1}) were dispensed onto the test line and control line, respectively, on the NC membrane by drawing a line with an Eppendorf tip. The membrane was then vacuum dried for 1h at room temperature to facilitate protein adsorption. The membrane was further blocked with PBS blocking buffer solution for 30 min and washed with 1 × PBS buffer to wash through any unconjugated antibodies. Finally, the nitrocellulose membrane was vacuum dried overnight and stored in a low relative humidity environment until use.

After preparation of the individual components, their assembly was carried out. A schematic of the fabricated prototype with its respective dimensions is shown in Fig. 1(c). Roller cutter was used to cut the nitrocellulose membrane of size 24 mm × 3 mm. The sample pad, conjugate pad, and absorbent pad were cut using a CO_2 laser beam machine. All parts were assembled on an adhesive hard plastic card to hold them in place. An overlapping of 2 mm was realized between the sample pad and conjugate pad, while conjugate pad and absorbent pad each were overlapped onto the nitrocellulose membrane with 1 mm to ensure proper flow of reagents through the test strip via capillary action.

I. Colorimetric detection of dengue NS1

For detection of dengue NS1, different concentrations of NS1 antigen (15, 25, 50, 100, and 250 ng mL^{-1}) were obtained by dilution of the stock NS1 solution (1.7 mg mL^{-1}) in PBS solution. Then, 150 μL of the prepared solutions was mixed with 150 μL of Au-rGO-Ab conjugate solution and stirred slowly for 5 min. Subsequently, 2 μL of capture antibody (0.1 μg mL^{-1}) was added and mixed thoroughly. The final volume was maintained at 0.5 mL and used for UV-vis spectroscopy measurements.

For detection of dengue NS1 on the developed lateral flow assay, different concentrations of NS1 were prepared using human serum as the buffer. Based on the previous literature, human serum was used to mitigate nonspecific adsorption and hence reduce false positives and demonstrate practical feasibility of the proposed assay.[35] Human blood was collected and centrifuged at 2000 rpm for 10 min to extract the serum. Further, 150 μL of prepared solutions of dengue NS1 with different concentrations (0, 3, 5, 10, 15, 25, and 50 ng mL^{-1}) was spiked into human serum and loaded onto the sample pads.

J. Signal intensity measurement

For color quantification, the paper strips were photographed with a mobile phone camera and the signal intensity was analyzed using ImageJ. Images were captured using a mobile phone camera to ensure objective data analysis to generate standardized data to be compared on a global basis.[36] The images were converted to 8-bit grayscale to acquire gray level intensities (lower intensity for darker pixels). A 12 × 250 pixels sq. region of interest was used to

assess the signal intensity. For each concentration, an average signal intensity at the test line was calculated by taking three replications. The normalized signal intensity (I_n) for each concentration of NS1 sample was calculated using the following equation, $I_n = (I_i - I_b)/(I_{max} - I_b)$, where I_b is the grayscale value of the blank, I_{max} is the grayscale value at the highest concentration, and I_i is the grayscale value at each sample concentration.

K. Limit of detection

The normalized signal intensity was plotted against different concentrations of NS1 and fit to a linear calibration curve. The limit of detection was calculated from the curve fit by using the formula $LOD = 3\sigma/m$, where σ is standard deviation of the response and m is the slope of the dose-response calibration curve.

III. RESULTS AND DISCUSSION

A. Nanocomposite characterization

The successful synthesis of Au-rGO was characterized by UV–Vis spectrometry. Figure 2(a) shows the UV-vis spectra of rGO and Au-rGO. For both the samples, rGO exhibits a strong absorption peak at 264 nm corresponding to π-π*transitions of C=C aromatic band. In addition, there is an emerging absorption peak at 529 nm for Au-rGO, corresponding to the characteristic surface plasmon resonance (SPR) band of AuNPs ensuring the successful loading of gold nanoparticles on the surface of rGO. Figure 2(b) shows the Raman spectra of rGO and Au-rGO. The two prominent peaks at 1348 and 1586 cm^{-1} in the rGO spectrum are attributed to the D and G peaks, respectively. The D-band is ascribed to the structural imperfections due to vibrations of sp^3 carbon atoms of disordered graphene nanosheets, while the G band arises from the tangential stretching mode of the E_2g phonons of the sp^2 carbon atom domains of graphite. In the case of Au-rGO, similar peaks at 1351 and 1591 cm^{-1} with higher intensities are observed. The removal of oxygenated groups during the synthesis of Au-rGO is confirmed by the higher value of the relative intensity ratios of the D and G bands (ID/IG = 1.10 for rGO

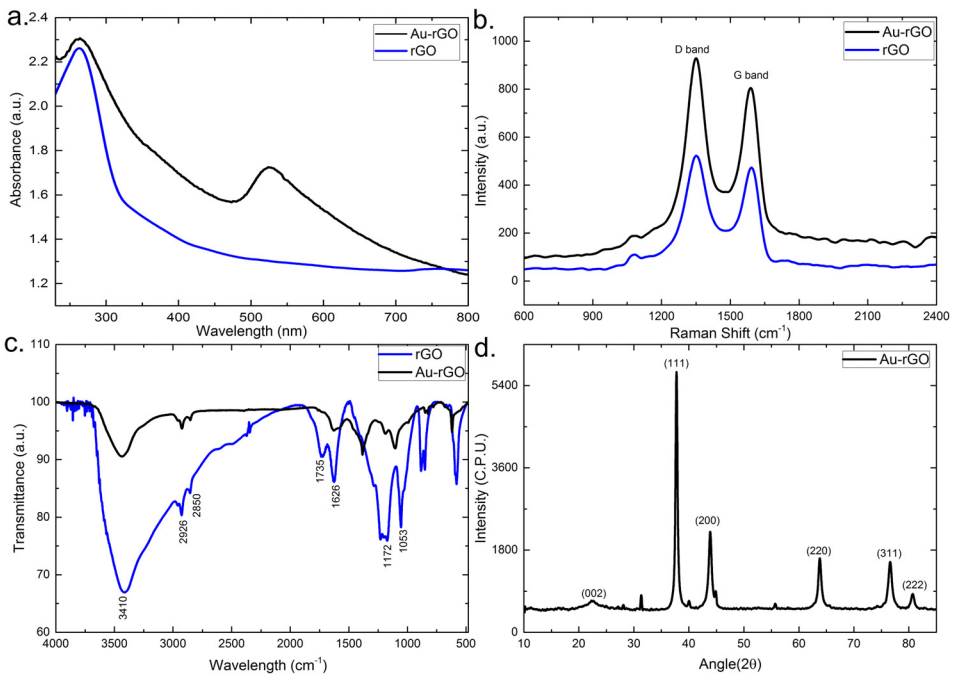

FIG. 2. Structural characterization of the as-synthesized nanocomposites. (a) UV-Vis spectra, (b) Raman spectra, (c) FTIR spectra of rGO and Au-rGO, and (d) XRD spectrum of Au-rGO.

and 1.12 for Au-rGO). Additionally in case of Au-rGO, the small red shift in the wavelength strongly suggests an interaction between gold nanoparticles and graphene. The functionalization of Au-rGO nanocomposites has also been examined by FTIR spectroscopy as shown in Fig. 2(c). FTIR spectra of rGO exhibit strong absorption bands at 3410, 1735, 1626, 1172, and 1053 cm^{-1} corresponding to the stretching vibrations from O-H, C=O carbonyl, C=C aromatic, C-O epoxy, and C-O alkoxy functional group. The absorption band at 2926 and 2850 cm^{-1} is assigned to the presence of CH2 bond. The FTIR spectrum of Au-rGO exhibits similar peaks as rGO, except for the decreased intensity at 1626 and 1102 cm^{-1}, corresponding to the COOH and C–OH groups.[37] This decrease in the intensity could be ascribed to AuNPs, consuming the oxygen groups present on the rGO sheets. The crystal structure of the final Au-rGO nanocomposite has further been investigated by XRD [Fig. 2(d)]. The rGO diffraction peak corresponding to (002) of the C plane appears at an angle of 22.29°, confirming the existence of a hexagonal structure. The diffraction peaks at (111), (200), (220), (311), and (222) can be attributed to the face centered cubic structure of Au (PDF 00-004-0783) displaying the crystallinity of AuNPs. The successful formation of nanocomposites has been further confirmed by analyzing the morphologies using transmission electron microscopy. The wrinkled and folded morphology of rGO is confirmed by the TEM image shown in Fig. 3(a). The inset shows the well-defined hexagonal diffraction pattern, confirming the crystalline structure of rGO sheet. The spherical AuNPs have shown an average size distribution of 40 nm [Fig. 3(b)]. Figure 3(c) shows TEM image of the Au-rGO nanocomposites, in which AuNPs are homogeneously dispersed on the surface of graphene sheet with an average size distribution of 39 nm. This minor reduction in the size of AuNPs substantiates the role of rGO in dispersion and stability of Au-rGO aqueous solution.[38] From the high-resolution TEM image of Au-rGO [Fig. 3(d)], the interplanar lattice spacing of AuNPs has been measured to be 0.237 nm corresponding to (111) plane in gold. This further suggests the crystalline nature of AuNPs embedded on the surface of graphene.

B. Characterization of Au-rGO-Ab conjugates

Figure 4(a) shows UV-vis spectra of the Au-rGO colloidal solution and of Au-rGO-Ab conjugates. A 3 nm red shift in the wavelength (529 to 532 nm) and broadening of the absorption

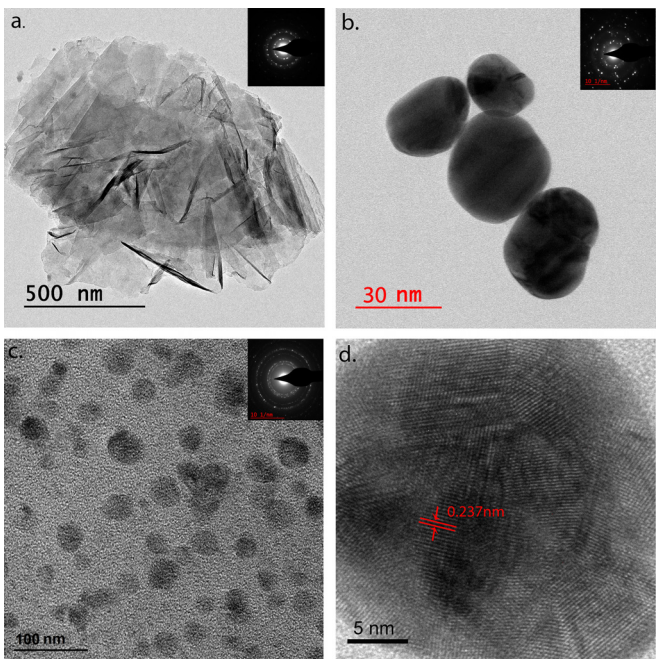

FIG. 3. TEM images of as-synthesized nanocomposites. (a) rGO, (b) AuNPs, (c) Au-rGO, and (d) High-resolution TEM of Au-rGO. Insets are respective SAED patterns.

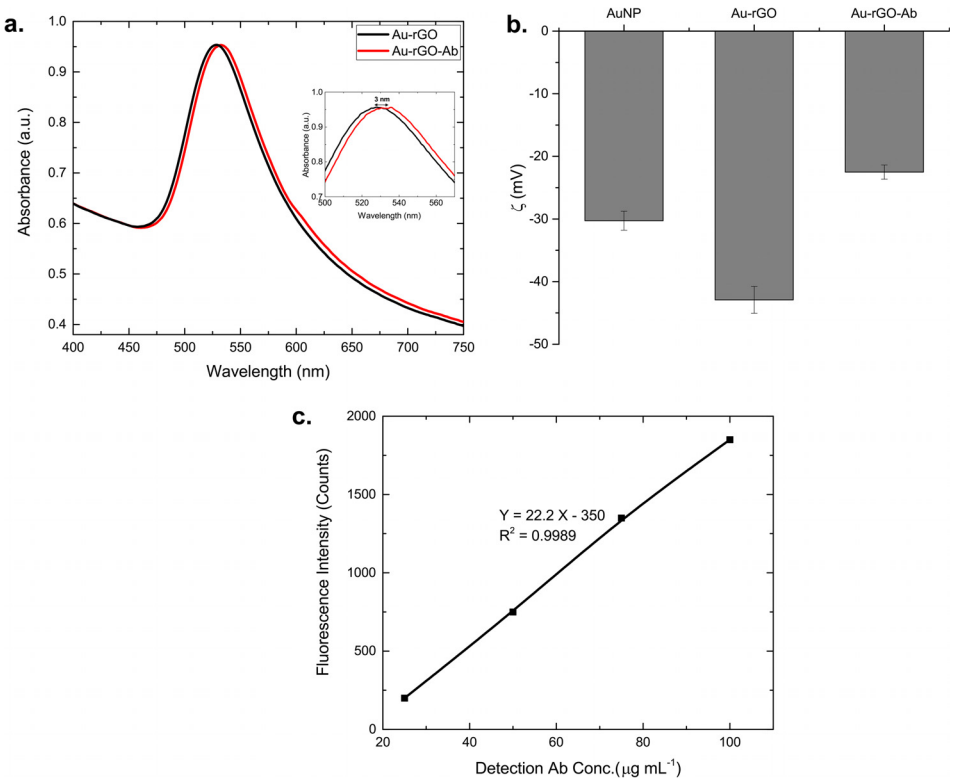

FIG. 4. Characterization of Au-rGO-Ab conjugates. (a) UV-Vis spectra and (b) zeta potential measurements of aqueous AuNPs, Au-rGO solution, and detection antibody conjugated Au-rGO. (c) Calibration curve of fluorescence vs. detection antibody concentration.

spectrum are observed as a result of the changes in the local refractive index after immobilization of antibodies on the surface of the nanoparticles. Further, stability of the AuNP, Au-rGO and Au-rGO-Ab samples has been confirmed by measurement of zeta potential as shown in Fig. 4(b). The zeta potential measurements reveal that all the samples demonstrate a negative surface charge with a zeta potential of -30 ± 1.5 mV, -43 ± 1.5 mV, and -22 ± 1.2 mV, respectively. The higher negative charge on Au-rGO implies a more stable solution compared to AuNP. Furthermore, a decrease in the surface charge after immobilization of antibodies suggests the successful conjugation of Au-rGO with the antibodies. Figure 4(c) shows the calibration curve of fluorescence intensity versus the FITC-labeled antibody concentration. A good linear relationship between fluorescence intensity and the FITC-labeled antibody concentration is observed with a correlation coefficient of 0.9989. The antibody loading on each nanoparticle is calculated to be 40.1 ± 8.5 Abs/NP. The average antibody footprint has thus been calculated to be 125.3 nm^2, based on the surface area of a nanoparticle as 5026.55 nm^2. The Ab footprint suggests a monolayer coverage, confirming successful directional conjugation of the antibodies over the nanoparticle surface.

C. Lateral flow immunoassay sensitivity enhancement

1. Au-rGO as detection label

In order to investigate the functionality of Au-rGO nanocomposite, the effect of detection label concentration was assessed using a conventional lateral flow assay (straight NC membrane). Au and Au-rGO were used as the labels, where the [Au] was kept identical. A similar trend was established for the two, where the test line signal intensity increased linearly with increasing concentration of detection label (Fig. S3). However, at the same concentration, Au-rGO exhibited a higher intensity signal compared to Au and achieved a threshold value at a

lower concentration. This can be attributed to the higher binding site capacity offered by Au-rGO for antibody immobilization.

Next, the straight lateral flow assay was tested for different NS1 concentrations (3, 5, 10, 15, 25, and 50 ng mL^{-1}). Photographs of the test strips are shown in Fig. S5(a). A grayscale analysis of the test line intensities led to the determination of detection limit to be 9.84 ng mL^{-1} [Fig. S5(b)]. This increased sensitivity compared to an assay utilizing Au as label[39] confirms the increase in nucleation sites due to rGO inhibiting the self-aggregation of AuNPs. This eventually allows more antibodies to react with the antigen to produce higher color density test lines leading to an approximately 5-fold increase in sensitivity. These results confirm that Au-rGO plays a significant role in signal enhancement, thereby improving the sensitivity of the assay.

2. Tapered NC membrane

The effect of taper angle on the sensitivity of the assay was established by testing immunoassay strips with varied taper angles. The signal intensity at the test line was quantified using ImageJ. The results indicated that the sensitivity increased with increasing taper angle, as evident from the decreasing grayscale value of the test line [Fig. S5(c), supplementary material]. However, the grayscale value started increasing after a taper angle of 0.9°. This increase can be attributed to the significant fluidic delay caused due to an increase in the flow resistance, leading to a decrease in the signal intensity. Therefore, an optimum taper angle of 0.9° was chosen for enhancing the detection limit of the assay.

D. Lateral flow immunoassay based detection of dengue NS1

The high sensitivity of the proposed detection scheme was first established in solution (Note S1). Having demonstrated detection of dengue NS1 in solution, we then tested our developed lateral flow immunoassay.

Figure 5(a) shows the photographs of paper strips after addition of different concentrations of NS1. The runtime of the assay was observed to be 10 min. The test line intensity was zero in the absence of NS1, while a distinguished test line was discerned in the presence of NS1. The visible color at the control line in each strip confirmed the successful run of the assay. It can be distinctly observed that the test strip was able to detect an NS1 concentration of 5 ng mL^{-1}, which was undetected by the straight strip.

The test line grayscale intensity was analyzed as a function of NS1 concentration using ImageJ (Sec. II).

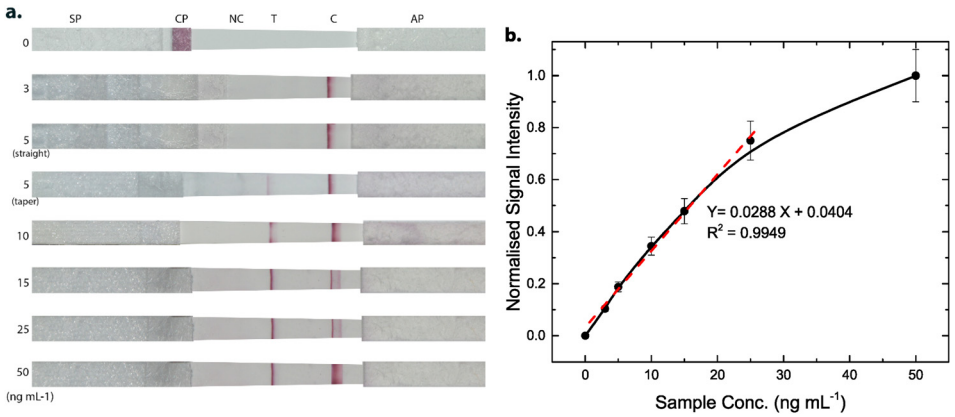

FIG. 5. (a) Photographs of tapered immunoassay strips after pipetting of dengue NS1 of different concentrations of 0, 3, 5, 10, 15, 25, and 50 ng mL^{-1} (from top-to-bottom). The third strip from the top shows a straight immunoassay strip at an NS1 concentration of 5 ng mL^{-1}. (b) Grayscale intensity curve for NS1 detection in the range of 0 to 50 ng mL^{-1}. Inset: linear calibration plot for NS1. Error bars (5%–8%) are shown for each data point.

Figure 5(b) illustrates the response curve of test line signal intensity at different NS1 concentrations. The normalized signal intensity was zero in the absence of NS1, indicating no non-specific binding to immobilized anti-NS1. The signal intensity was further observed to increase with the increasing concentration of NS1. The normalized signal intensity of the test line varied linearly between 3 and 25 ng mL^{-1} with a linear regression equation, $Y = 0.0288X + 0.0404$, where X is the NS1 concentration and Y is the normalized signal intensity. The LOD was calculated to be 4.90 ng mL^{-1} ($R^2 = 0.9949$), which is the lowest detection limit reported till date (100 μg mL^{-1},[40] 150 ng mL^{-1},[10] and 55.3 ng mL^{-1} [39]). This low detection limit suggests that our device can be used to detect NS1 in human serum at a concentration of clinical relevance, i.e., 50 μg mL^{-1}.[41] Further, to investigate the binding affinity of Au-rGO-Ab-Ag complex and capture antibody, modified Langmuir model was employed. The effective binding affinity constant (K_D^{eff}) was obtained to be 0.98 nM.[35] Such a low K_D^{eff} value implies an excellent binding affinity of the antibody-antigen interaction.

E. Validating the immunoassay point-of-care diagnostic device using clinical serum samples

To validate the feasibility of the proposed lateral flow assay in actual samples, the paper device was employed for detecting Dengue in real human serum samples. First, the collected blood samples were centrifuged for 10 min at 2000 rpm to extract the serum. The serum samples were then dispensed on the sample pad and the assay was run. As shown in Fig. 6(a), the assay tested positive for Dengue NS1 samples of different serotypes, whereas it is negative for Dengue IgG and IgM samples. This suggests the good reliability and accuracy of the proposed lateral flow device for Dengue NS1 detection in real human blood samples.

F. Specificity and stability

The specificity of the prepared lateral flow device was probed by testing the strip for different samples of dengue NS1 (serotype 1 and 2), dengue IgG, and Malaria parasite plasmodium vivax at a concentration of 50 ng mL^{-1}. As is evident from the graph in Fig. 6(b), the assay exhibited a positive signal for only dengue NS1 samples. The signal intensity on the test line

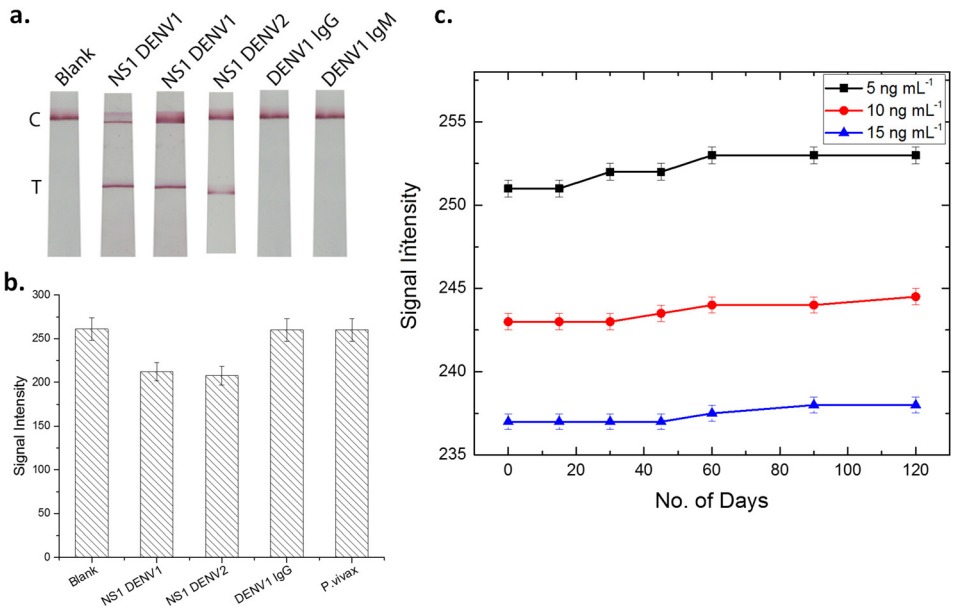

FIG. 6. (a) Photograph of test strip: blank and after addition of NS1 DENV1, NS1 DENV1, DENV1 IgG, and IgM. (b) Specificity of lateral flow immunoassay for detection of NS1. The histogram shows the colorimetric response to various samples. (c) Long-term stability test of paper-based device at room temperature.

for samples other than NS1 is analogous to that of the blank sample. These results suggest that the strips are specific in detecting recombinant dengue NS1 protein without any cross-reactive interference, confirming the high specificity of the assay.

Next, to assess the long-term stability of the lateral flow device, the prepared strips were stored at room temperature under dry conditions. After 15, 30, 45, 60, 90, and 120 days of storage, the devices were tested using different concentrations of NS1 (5, 10, and 15 ng mL^{-1}). The color readout was visually inspected and quantitatively measured using a grayscale method as described earlier. As shown in Fig. 6(c), no significant change in the signal intensity was observed even after 4 months (minor change of ∼1%). This is indicative of the adequate stability and robustness of the developed device.

IV. CONCLUSIONS

We propose a novel lateral flow immunoassay that uses a tapered NC membrane and Au-rGO as a detection label for highly sensitive detection of dengue NS1. Exploiting Au-rGO nanocomposites presented the dengue antigen with increased nucleation sites illustrating high sensitivity of the assay. In addition, with an optimum taper angle of 0.9°, the concentration gradient at the test line could be tuned to achieve an 11-fold improvement in the detection limit. The device features a high sensitivity (4.9 ng mL^{-1}), low runtime (10 min), and a simple manufacturing process over the previously existing devices. The developed device has the potential to aid in rapid diagnosis for implementation of proper healthcare measures to prevent severe complications. This proof-of-concept device could be used in future for differential diagnosis of infections with indistinguishable clinical manifestations, like malaria, Zika, chikungunya, etc. Furthermore, several developed mobile-based readers could be integrated with the device for quantitative measurements at concentrations too low to be read by eye.

SUPPLEMENTARY MATERIAL

See supplementary material for the plot of effect Au-rGO complex on the test line signal intensity, solution based detection of dengue NS1, and detection of dengue NS1 on straight immunoassay strips.

ACKNOWLEDGMENTS

This work was supported by the Ministry of Human Resource Department (MHRD), India, under the Design Innovation Centre (DIC) scheme (Project No. MHRD/DESP/2016142H).

[1]R. W. Peeling, H. Artsob, J. L. Pelegrino, P. Buchy, M. J. Cardosa, S. Devi, D. A. Enria, J. Farrar, D. J. Gubler, and M. G. Guzman, Nat. Rev. Microbiol. **8**, S30–S37 (2010).
[2]P. R. Young, P. A. Hilditch, C. Bletchly, and W. Halloran, J. Clin. Microbiol. **38**(3), 1053–1057 (2000).
[3]M. G. Guzman, S. B. Halstead, H. Artsob, P. Buchy, J. Farrar, D. J. Gubler, E. Hunsperger, A. Kroeger, H. S. Margolis, and E. Martínez, Nat. Rev. Microbiol. **8**, S7–S16 (2010).
[4]E. A. Henchal and J. R. Putnak, Clin. Microbiol. Rev. **3**(4), 376–396 (1990).
[5]S. Alcon, A. Talarmin, M. Debruyne, A. Falconar, V. Deubel, and M. Flamand, J. Clin. Microbiol. **40**(2), 376–381 (2002).
[6]R. S. Lanciotti, C. H. Calisher, D. J. Gubler, G.-J. Chang, and A. V. Vorndam, J. Clin. Microbiol. **30**(3), 545–551 (1992).
[7]P. Dussart, B. Labeau, G. Lagathu, P. Louis, M. R. Nunes, S. G. Rodrigues, C. Storck-Herrmann, R. Cesaire, J. Morvan, and M. Flamand, Clin. Vaccine Immunol. **13**(11), 1185–1189 (2006).
[8]W. R. Wong, S. D. Sekaran, F. R. M. Adikan, and P. Berini, Biosens. Bioelectron. **78**, 132–139 (2016).
[9]P. D. Sinawang, V. Rai, R. E. Ionescu, and R. S. Marks, Biosens. Bioelectron. **77**, 400–408 (2016).
[10]C.-W. Yen, H. de Puig, J. O. Tam, J. Gómez-Márquez, I. Bosch, K. Hamad-Schifferli, and L. Gehrke, Lab Chip **15**(7), 1638–1641 (2015).
[11]J. O. Tam, H. de Puig, C.-W. Yen, I. Bosch, J. Gómez-Márquez, C. Clavet, K. Hamad-Schifferli, and L. Gehrke, J. Immunoassay Immunochem. **38**, 355 (2017).
[12]S.-J. Lo, S.-C. Yang, D.-J. Yao, J.-H. Chen, W.-C. Tu, and C.-M. Cheng, Lab Chip **13**(14), 2686–2692 (2013).
[13]Y. Zhang, J. Bai, and J. Y. Ying, Lab Chip **15**(6), 1465–1471 (2015).
[14]J. R. Choi, J. Hu, S. Wang, H. Yang, W. A. B. Wan Abas, B. Pingguan-Murphy, and F. Xu, Crit. Rev. Biotechnol. **37**, 100 (2016).
[15]M. Arruebo, M. Valladares, and Á. González-Fernández, J. Nanomater. **2009**, 439389 (2009).
[16]C. D. Medley, J. E. Smith, Z. Tang, Y. Wu, S. Bamrungsap, and W. Tan, Anal. Chem. **80**(4), 1067–1072 (2008).
[17]D. M. Cate, J. A. Adkins, J. Mettakoonpitak, and C. S. Henry, Anal. Chem. **87**(1), 19–41 (2015).

[18]S. Chaterji, J. C. Allen, Jr., A. Chow, Y.-S. Leo, and E.-E. Ooi, Am. J. Trop. Med. Hyg. **84**(2), 224–228 (2011).
[19]Y. Song, Y. Chen, L. Feng, J. Ren, and X. Qu, Chem. Commun. **47**(15), 4436–4438 (2011).
[20]L.-N. Zhang, H.-H. Deng, F.-L. Lin, X.-W. Xu, S.-H. Weng, A.-L. Liu, X.-H. Lin, X.-H. Xia, and W. Chen, Anal. Chem. **86**(5), 2711–2718 (2014).
[21]K. P. Loh, Q. Bao, P. K. Ang, and J. Yang, J. Mater. Chem. **20**(12), 2277–2289 (2010).
[22]J. R. Choi, Z. Liu, J. Hu, R. Tang, Y. Gong, S. Feng, H. Ren, T. Wen, H. Yang, and Z. Qu, Anal. Chem. **88**(12), 6254–6264 (2016).
[23]L. Rivas, M. Medina-Sánchez, A. de la Escosura-Muñiz, and A. Merkoçi, Lab Chip **14**(22), 4406–4414 (2014).
[24]R. Tang, H. Yang, Y. Gong, Z. Liu, X. Li, T. Wen, Z. Qu, S. Zhang, Q. Mei, and F. Xu, Sci. Rep. **7**(1), 1360 (2017).
[25]S. Kumar, P. Bhushan, and S. Bhattacharya, Anal. Methods **8**(38), 6965–6973 (2016).
[26]N. R. Jana, L. Gearheart, and C. J. Murphy, Langmuir **17**(22), 6782–6786 (2001).
[27]S. Kumar, J. Aaron, and K. Sokolov, Nat. Protoc. **3**(2), 314–320 (2008).
[28]H. de Puig, S. Federici, S. H. Baxamusa, P. Bergese, and K. Hamad Schifferli, Small **7**(17), 2477–2484 (2011).
[29]S. Qian and H. H. Bau, Anal. Biochem. **322**(1), 89–98 (2003).
[30]M. Gudmundsson and A. Bjelle, Angiology **44**(5), 384–391 (1993).
[31]L. T. Sniegoski and J. R. Moody, Anal. Chem. **51**(9), 1577–1578 (1979).
[32]C. S. Brooks and W. R. Purcell, Petroleum Trans., AIME **195**, 289–296 (1952).
[33]C. Parolo, M. Medina-Sánchez, A. de la Escosura-Muñiz, and A. Merkoçi, Lab Chip **13**(3), 386–390 (2013).
[34]J. Romero and O. Gonz, Int. J. Pure Appl. Math. **82**(1), 41–52 (2013).
[35]H. de Puig, I. Bosch, M. Carré-Camps, and K. Hamad-Schifferli, Bioconjugate Chem. **28**(1), 230 (2017).
[36]I. Bosch, H. de Puig, M. Hiley, M. Carré-Camps, F. Perdomo-Celis, C. F. Narváez, D. M. Salgado, D. Senthoor, M. O'grady, and E. Phillips, Sci. Transl. Med. **9**(409), eaan1589 (2017).
[37]H. Zhang, D. Hines, and D. L. Akins, Dalton Trans. **43**(6), 2670–2675 (2014).
[38]M. Liu, H. Zhao, S. Chen, H. Yu, and X. Quan, ACS Nano **6**(4), 3142–3151 (2012).
[39]M. Sánchez-Purrà, M. Carré-Camps, H. de Puig, I. Bosch, L. Gehrke, and K. Hamad-Schifferli, ACS Infect. Dis. **3**(10), 767–776 (2017).
[40]H. K. Wang, C. H. Tsai, K. H. Chen, C. T. Tang, J. S. Leou, P. C. Li, Y. L. Tang, H. J. Hsieh, H. C. Wu, and C. M. Cheng, Adv. Healthcare Mater. **3**(2), 187–196 (2014).
[41]S. Watanabe, K. H. Tan, A. P. Rathore, K. Rozen-Gagnon, W. Shuai, C. Ruedl, and S. G. Vasudevan, J. Virol. **86**(10), 5508–5514 (2012).